Clin Exp Metastasis (2008) 25:581–590
DOI 10.1007/s10585-008-9175-1

RESEARCH PAPER

Intraosseous injection of RM1 murine prostate cancer cells promotes rapid osteolysis and periosteal bone deposition

N. Patrick McCabe · Maria Madajka · Amit Vasanji · Tatiana V. Byzova

Received: 15 August 2007 / Accepted: 26 April 2008 / Published online: 28 May 2008

Abstract The molecular mechanisms associated with prostate cancer (PCa) progression within bone remain a topic of intense investigation. With the availability of transgenic mouse strains, a model of PCa for use in immune competent/transgenic mice would be highly beneficial. This study was designed to explore the utility of RM1 mouse PCa cells in investigations of tumor:bone interactions. The efficacies of several implantation techniques were examined for reliably producing intra-bone RM1 tumor growth and bone lesion formation in immune competent mice. Longitudinal monitoring of bone remodeling and lesion phenotypes was conducted by microcomputed tomography (μCT) and histological analyses. Our results indicate that direct intrabone injections of RM1 cells are necessary for tumor growth within bone and direct implantation promotes the rapid development of osteolytic bone lesions with periosteal bone deposition post-cortical breach. In vitro, RM1 cells promote the proliferation of osteoblast (MC3T3-E1) and osteoclast (Raw264.7) progenitors in a dose dependent manner. Conditioned culture media from RM1 cells appears to promote earlier expression of genes/proteins associated with osteoblastic differentiation. While clearly stimulating osteoclast function in vivo, RM1 cells had little effect on differentiation and tartate resistant acid phosphatase (TRAP) expression by Raw264.7 cells. These data, coupled with in vivo μCT images, indicate the ability of RM1 cells to induce mixed, yet predominentally osteolytic, responses in bone and illustrate the potential of RM1 cells as a model of investigating prostate tumor:stroma interactions in immune competent/transgenic mice on a C57BL/6 background.

Keywords Prostate cancer · Bone · Animal model · Osteolytic · Osteoblastic

Introduction

In 2007, it is estimated that approximately 220,000 new cases of prostate cancer will be reported in the United States [1] making it the most common form of cancer in men. Individuals with advanced disease are commonly afflicted with metastases to secondary sites, of which the skeletal compartment predominates [2] leading to substantial bone pain and mortalities. Although the nature of bone metastatic prostate cancer lesions have been described as osteoblastic, these lesions develop concomitantly with notable amounts of bone resorption [3]. While the topic of intense investigation, factors contributing to the stimulation of such bone remodeling phenotypes still remain largely unidentified.

The paucity of effective, clinically relevant in vivo models has limited the expansion of knowledge regarding the interplay between prostate cancer cells and the bone

Electronic supplementary material The online version of this article (doi:10.1007/s10585-008-9175-1) contains supplementary material, which is available to authorized users.

N. P. McCabe · M. Madajka · T. V. Byzova (✉)
Department of Molecular Cardiology, NB50, The Cleveland Clinic Lerner Research Institute, Cleveland, OH 44195, USA
e-mail: byzovat@ccf.org

A. Vasanji
Department of Biomedical Engineering, The Cleveland Clinic Lerner Research Institute, Cleveland, OH, USA

T. V. Byzova
The Cleveland Clinic, Taussig Cancer Center, Cleveland, OH, USA

microenvironment. The use of xenotransplantation models has proven effective and yielded substantial data covering many facets of prostate carcinogenesis including bone metastases. Unfortunately, these models of bone metastatic cancers incompletely represent tumor:bone stroma interactions due to a lack of host immune responses and potential tumor/host incompatibilities of biological factors, such as cell adhesion molecules/cognate receptors or growth factors and their receptors. The development of murine prostate cancer models, however, is severely hindered by a lack of spontaneous tumor development within the mouse prostate. Several models of murine prostate cancer exist, including those generated through the use of prostate tissue specific promoters to drive expression of the SV40 small t and/or large T antigens [4, 5], or the development of transgenics with conditional knockouts [6] or hemizygous knockouts [7]. Another model, the mouse prostate reconstitution model (MPR) developed by retroviral infection of murine urogenital sinus for the expression of activated oncogenes [8], has been effectively used in immunotherapy studies of prostate cancer [9, 10]. Cell lines developed using the MPR model are highly tumorigenic in mice and several cell lines have been characterized that spontaneously metastasize [11].

In this study, we describe the use of RM1 cells (developed using the MPR model and syngeneic to C57BL/6 mice) as a new model for studying the interactions between prostate cancer cells and bone stroma. We have determined the most effective injection method and optimal cell numbers to yield reproducible skeletal lesions and describe the resultant lesion phenotypes. In addition, we begin to characterize the ability of RM1 cells to stimulate differentiation of osteoblast and osteoclasts precursors in vitro.

Methods

Cell culture

The RM1 murine prostate cancer cell line was provided by W. Heston (Cleveland Clinic). These cells were originally generated from C57BL/6 mice using the mouse prostate reconstitution model (MPR) [8] with cells characterized by Baley et al. [12]. Cells were cultured in vitro in RPMI 1640 supplemented with 10% (v/v) heat inactivated fetal bovine serum (FBS), 100 U/ml penicillin, 100 μg/ml streptomycin and regularly passaged by trypsinization (0.05% (v/v) trypsin, 0.53 mM EDTA). Conditioned culture media (CCM) from RM1 cells was obtained as follows: RM1 cells were grown to 70% confluence and washed 2× in PBS. Media was replaced with FBS and antibiotic free RPMI. Conditioned media was collected 24 h later and concentrated in Amicon Ultra centrifugal filter devices with a 5 k MWCO (Millipore, Billerica, MA). Concentrated media was frozen at −80°C until use.

The preosteoblastic cell line, MC3T3-E1 was kindly provided by Dr. Ron Midura (Cleveland Clinic). MC3T3-E1 cells were early passage (passage 7) and were maintained in ascorbic acid (AA) free αMEM (Invitrogen, Carlsbad, CA) containing 10% FBS. Raw264.7 cells were from ATCC (Manassa, Va) and were maintained in DMEMF12 containing 10% FBS, 100 U/ml penicillin and 100 μg/ml streptomycin.

Tumor cell implantations

Mice (C57BL/6) were anesthetized intraperitoneal (IP) with ketamine (100 mg/kg) and xylazine (10 mg/kg) directly before surgical intervention. RM1 cell injections (1.0×10^3–3.0×10^6 cells in PBS) were performed according to the following procedures:

Injection into the femoral artery

All hair from the upper side of the left hindlimb was removed with clippers and the skin cleaned with a chlorohexidine solution. A unilateral 1.0 cm incision was made over the left medial thigh exposing the femoral artery. A ligature was performed 0.5 cm proximal to the bifurcation of the femoral artery. Two additional ligatures were placed on the deep bridge and collateral arteries 3.0 mm proximal to the bifurcation. A 29G insulin syringe was inserted into the femoral artery and RM1 cells were introduced.

Intracardiac injection

Anesthetized mice were positioned on their back and the chest area was rinsed with ethanol. Both upper limbs were lifted in order to expose the chest and locate the heart externally via the apex beat. A 29G insulin syringe was inserted slowly into the left ventricle, and the injection of RM1 cells was performed.

Intratibial injections

Mice were injected intratibially with RM1 cells in 10 μl PBS. Briefly, mice were anesthetized by IP injection with ketamine/xylazine, the injection site was shaven then prepped with a chlorhexidine solution. The knee was flexed and a 27G tuberculin syringe was used to bore a hole into the proximal end of the right tibia and then replaced with a 29G insulin syringe containing the cell solution for implantation. The contra lateral tibia was injected with PBS alone to act as a control for injury induced remodeling of bone.

Microcomputed tomography

Anesthetized mice (ketamine/xylazine mixture) were placed on the scanning platform of a GE eXplore Locus μCT (GE Healthcare, Piscataway, NJ) and 360 X-ray projections were collected in 1° increments (80 kVp; 500 mA; 26 min total scan time). Projection images were preprocessed and reconstructed into 3-dimensional volumes (1024^3 voxels, 20 μm resolution) on a 4PC reconstruction cluster using a modified tent-FDK cone-beam algorithm (GE reconstruction software). Three-dimensional data was processed and rendered (isosurface/maximum intensity projections) using MicroView (GE Healthcare).

Histology

Injected tibiae were fixed and decalcified overnight in Decalcifier I solution (Surgipath, Richmond, IL), cut longitudinally and incubated overnight again in Decalcifier I. Tissue was then embedded in paraffin and sectioned (5 μm). Sections were stained with hematoxylin and eosin (H&E). Visualization and imaging were done using a Leica DM 2500 microscope (Leica Microsystems GmbH, Wetzlar, Germany) and Retiga EXi camera (Q Imaging, Surrey, BC Canada).

Cell proliferation

MC3T3-E1 cells were plated in 96-well plates at a density of 100 cells/well in AA free αMEM with 10% FBS in triplicate for each timepoint. Raw264.7 cells (100 cells/well) were similarly plated in 96 well plates in DMEMF12 with 10% FBS. Cell proliferation was monitored by the CYQUANT NF cell proliferation assay (Invitrogen) and a CYTOFLUOR II fluorescence multi-well plate reader (PerSeptive Biosystems, Framingham, MA). One day following seeding of cells, media was replaced with fresh media alone or media spiked with 10, 50, or 100 μg/ml RM1 conditioned culture media (CCM). Cell numbers were determined 72 h post-treatment.

Osteoclast differentiation

Raw264.7 cells in DMEMF12 w/10% FBS were plated at 1.5×10^5 cells/cm^2 in wells of a 96 well plate. Media was replaced the following day with fresh complete DMEMF12 media alone, complete media with supplemental RANKL (R&D Systems, Minneapolis, MN) at 100 ng/ml, complete media with RM1 conditioned culture media at various concentrations, or complete media with supplemental RANKL (100 ng/ml) and RM1 conditioned culture media. All media was replaced on day 3 with fresh media with the constituents listed above. On the sixth day following initiation of treatment, cells were stained for TRAP (Sigma; 387A) and cells containing >3 nuclei were counted.

Semi-quantitative RT-PCR

MC3T3-E1 cells were plated in 12 well plates (5×10^4 cells/well) and grown to confluence. Media was then replaced with fresh AA free αMEM with 10% FBS, osteogenic supplement (OS) media (αMEM with 10% FBS plus 50 μg/ml AA and 10 mM β-glycerolphosphate), AA free αMEM with 10% FBS plus RM1 CCM (50 μg/ml), or OS media plus RM1 CCM (50 μg/ml). Media was changed every 3 days following up to 15 days. Total RNA was isolated using TRIzol Reagent (Invitrogen) and 1 μg was reverse transcribed using Thermoscript RT (Invitrogen) and oligo dT primers. Primers for PCR were designed using Primer3 [13] and were as follows: bone sialoprotein (BSP); forward, 5′-AAAGTGAAGGAAAGCGACGA-3′, reverse, 5′-GTTCCTTCTGCACCTGCTTC-3′ (amplicon: 215 bp), collagen type Iα1 (ColIα1): forward, 5′-GAGCGGAGAGTACTGGATCG-3′, reverse, 5′-GCTTCTTTTCCTTGGGGTTC-3′ (amplicon:158 bp), β actin; forward, 5′-TGTTACCAACTGGGACGACA-3′, reverse, 5′-GGGGTGTTGAAGGTCTCAAA-3′ (amplicon: 165 bp). PCR was carried out as follows: 94°C for 5 min followed by 22 (BSP), 20 (ColIα1), or 30 (β actin) cycles at 94°C for 30 s, 55°C for 30 s, and 72°C for 30 s. The resultant PCR products were visualized on 2% (w/v) agarose gels. Band densitometry was performed using Photoshop CS3 Extended (Adobe Systems, Inc., San Jose, CA).

Detection of alkaline phosphatase

MC3T3-E1 cells (passage 7) were plated at 1×10^4 cells/cm^2 in the wells of a 24 well plate in αMEM with 10% FBS. The following day, media was replaced with αMEM (2% FBS), αMEM (2% FBS) plus 50 μg/ml AA and 10 mM β-glycerolphosphate, αMEM (2% FBS) plus RM1 CCM (50 μg/ml), or αMEM (2% FBS) plus 50 μg/ml AA and 10 mM β-glycerolphosphate and RM1 CCM (50 μg/ml). All media was refreshed on day 3 and surface expression of alkaline phosphatase (ALP) was detected on day 5 using the One-Step NBT/BCIP solution from Pierce (Rockford, IL). Briefly, cells were washed 3× in calcium and phosphate free saline, fixed for 30 min at room temperature in paraformaldehyde (4% w/v), washed 3× dH_2O, then stained with the One-Step NBT/BCIP solution at room temperature for 15 min. Staining was photographed using a Leica DMIRB microscope (Leica) with attached Retiga SRV camera (Q Imaging). Images were analyzed using Image Pro Plus (v5.1).

Quantificatin of serum TRAP 5b

RM1 cells (1×10^3) were injected into the tibia of twelve week old female C57BL/6 mice. Mice injected with PBS only were used as controls. Two weeks following implantation, blood was collected and serum separated. The levels of TRAP 5b in serum of mock and RM1 injected mice were determined using an ELISA (MouseTRAP Assay; Immunodiagnostic Systems Inc., Fountain Hills, AZ).

Statistical analysis

Analysis of Variance (one-way) with Dunnett's (proliferation, osteoclast differentiation) or Bonferroni post-tests was used to analyze the statistical significance of experimental results. Differences in serum TRAP were determined by student's *t* test. Results were considered significant when *P* values were less than 0.05.

Results

Injections, cell quantities, and time course of RM1 induced bone lesions

Our goal with this work was to explore the potential of a new model for investigating prostate cancer:bone interactions in immune competent/transgenic C57BL/6 mice. For this purpose, we have chosen to use the RM1 cell line [8, 12]. RM1 mouse prostate cancer cells rapidly proliferate in culture and form large subcutaneous tumors (data not shown) leading us to suspect that they would thrive in a nutrient rich environment such as bone. Several different injection methods were examined to find the most reliable and reproducible technique for developing bony lesions. As shown in Table 1, the injection methods and cell quantities tested included introduction of cells into the femoral artery for site specific bone metastases (hind limb), intracardiac inoculation for nonspecific bone metastases, and direct delivery of cells to bone (tibia). A complete lack of bone metastases was noted upon delivery of RM1 cells into the femoral artery or by intracardiac injection 21 days following injection, regardless of the quantity of cells introduced. Large tumors had formed adjacent to these injection sites by 21 days, thus precluding the discovery of metastases at later time points. It appears that even minimal leakage of RM1 cells into soft tissues at injection sites results in local tumor formation.

Following direct intraosseous implantation, RM1 cells reliably produced bony lesions in all animals (19/19) independent of injected cell quantity. To longitudinally monitor bone lesion development following RM1 cell injection (1×10^3 cells), the hind limbs of injected mice were imaged using a μCT scanner at 1, 5, 10, 15, and 20 days following implantation. Representative three dimensional isosurface reconstructions, single slice X-ray projections, and maximum intensity projections (MIP) of a single mouse are shown in Fig. 1. As early as 5 days, the injection site was walled off with new bone (slice view) that extended into the tibial metaphysis. New bone in the metaphysis was resorbed by 10 days with an accompanying hole found in the anterior cortex (3D view). Cortical resorption increased at 15 and 20 days and is apparent in 3D volumes, single slices, and MIPs. Three dimensional isosurface renderings also indicate regions of periosteal bone deposition by 20 days following RM1 cell injection.

Table 1 Determination of injection site, cell quantities, and tumor incidence of experimental bone metastases of RM1 cells

Injection site	Cell quantity	Tumor incidence
Femoral artery[a]	3.0×10^6	0/4
	1.5×10^6	0/5
	5.0×10^5	0/4
	2.5×10^5	0/7
	4.0×10^4	0/6
	2.0×10^4	0/3
Intracardiac[a]	3.0×10^5	0/4
	1.5×10^5	0/3
Intratibial	2.5×10^5	5/5
	1.0×10^4	4/4
	1.0×10^3	10/10

[a] Soft tissue tumors formed at site of injection due to cell spillage

Gross and histologic examination of RM1 injected tibiae

All animals injected intratibially with RM1 cells formed soft tissue tumors adjacent to bone that were grossly visible by 15 days. Figure 2a depicts a soft tissue tumor adjacent to bone typical for all injections after 21 days. Histological specimens of tibia injected with RM1 cells (1×10^4 and 1×10^3) are shown in Fig. 2b and c, respectively. Fourteen days following the intratibial implantation of 1×10^4 RM1 cells, normal marrow cells of the tibial metaphysis were displaced and sections of cortical bone were eroded exposing the periosteum. Invasion of adjacent muscle tissue was also evident. Reducing the cell quantity to 1×10^3 had the potential to slow this process and led to tumor nests within the tibial metaphysis in some animals 14 days following implantation (Fig. 2c).

Three dimensional reconstructions of 2D image projections from μCT scans acquired 21 days following intratibial implantation of 1×10^3 RM1 cells illustrate the

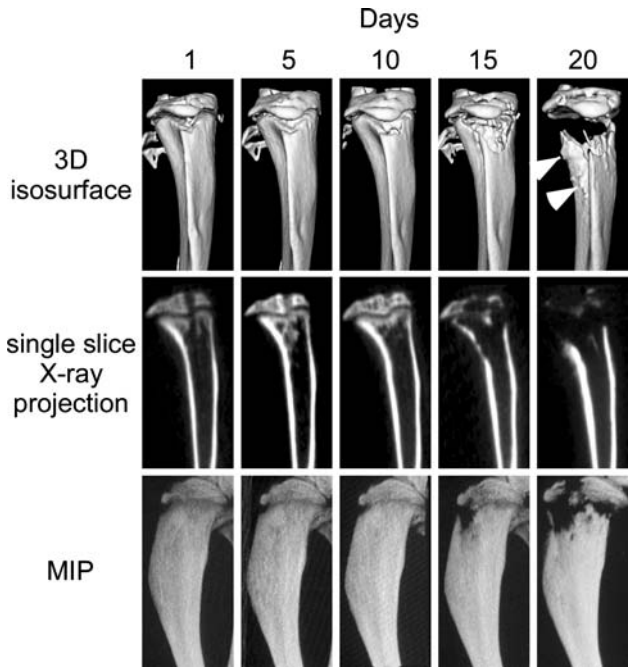

Fig. 1 Longitudinal evaluation of RM1 induced bone lesion development using μCT. RM1 cells (1×10^3) were injected directly into the tibia of anesthetized C57BL/6 mice. Injected tibiae were subjected to μCT analyses 1 day post-implantation of RM1 cells and at 5 day intervals up to 20 days post-implantation. Top row depicts 3D isosurface reconstructions of μCT data in an anterior–posterior view. A hole in the cortical bone of the tibia appears as early as 10 days and becomes progressively larger. At 20 days, new bone (arrowheads) deposits are visible on the periosteal surface. Middle row depicts individual X-ray projections that bisect the injection site. Bottom row depicts maximum intensity projections (MIPs) of the injected tibia. All images from the three rows are of the same (registered) tibia monitored for a period of 20 days

osteolytic nature of bone residing RM1 tumors, while small foci of periosteal bone deposition are evident (Fig. 3b). A normal tibia is shown for comparison in Fig. 3a. Histological examination indicated that RM1 cells can illicit periosteal responses consisting of both irregular, random bone deposition (Fig. 3c) and cortical thickening (Fig. 3d). In regions of new bone, there was a notable presence of bone resorbing osteoclasts. Figure 3e shows a mock injected tibia 10 days following surgical intervention with no discernable presence of osteoclasts lining the endosteal surface of the tibia. Stimulation of osteoclast recruitment to the endosteal suface (Fig. 3f) was apparent at earlier time points where RM1 cells had not yet breached the tibial cortex.

Osteoclast and osteoblast proliferation and maturation

Our uCT images clearly indicate the ability of RM1 cells to promote osteoclast function leading to robust tibial lysis. Elevated osteoclast function was confirmed in vivo by determining the levels of TRAP in serum of RM1 injected mice compared to mock injected mice (Fig. 4a). To test other functions associated with the development of osteolytic lesion formation such as proliferation and maturation of osteoclast progenitors, we treated Raw264.7 cells (monocyte/macrophage lineage) with various concentrations of RM1 CCM. As shown in Fig. 4b, RM1 CCM enhanced Raw264.7 cell proliferation at low concentrations (5 μg/ml) and had little to no effect at concentrations up to 50 μg/ml. Expression of TRAP was not inhibited at any tested concentration of RM1 CCM in the presence of RANKL while RM1 CCM alone was unable to stimulate TRAP expression (Fig. 4c, d). Interestingly, higher concentrations of RM1 conditioned culture media inhibited the ability of Raw264.7 cells to form multinucleate TRAP expressing cells.

Since we found that intraosseous implantation of RM1 cells can promote periosteal bone deposition, we decided to test whether RM1 prostate cancer cells can promote osteoblast progenitor proliferation and differentiation. For this purpose, we investigated the effects of RM1 CCM on the proliferation and maturation of osteoblast precursor

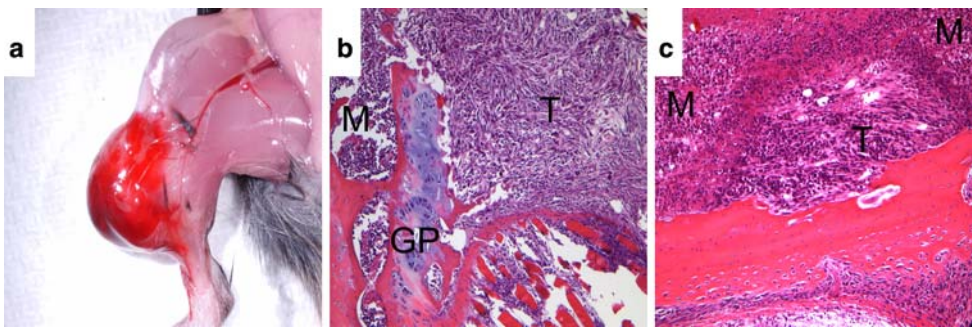

Fig. 2 Gross and histological examination of RM1 injected tibia. (**a**) Gross analysis and (**b**) H&E stained section of a tibia 14 days following the implantation of 1×10^4 RM1 cells. In (**b**), note that RM1 cells (T) have displaced the marrow of the tibial metaphysis and promoted extensive cortical lysis, subsequently invading adjacent soft tissue. Growth plate (GP) and marrow (M) of the epiphysis are indicated. Magnification of 10×. (**c**) H&E stained section of tibia 14 days following the injection of 1×10^3 RM1 cells. A tumor nest (T) is shown adjacent to an area of focal cortical lysis and surrounded by marrow (M). Magnification of 20×

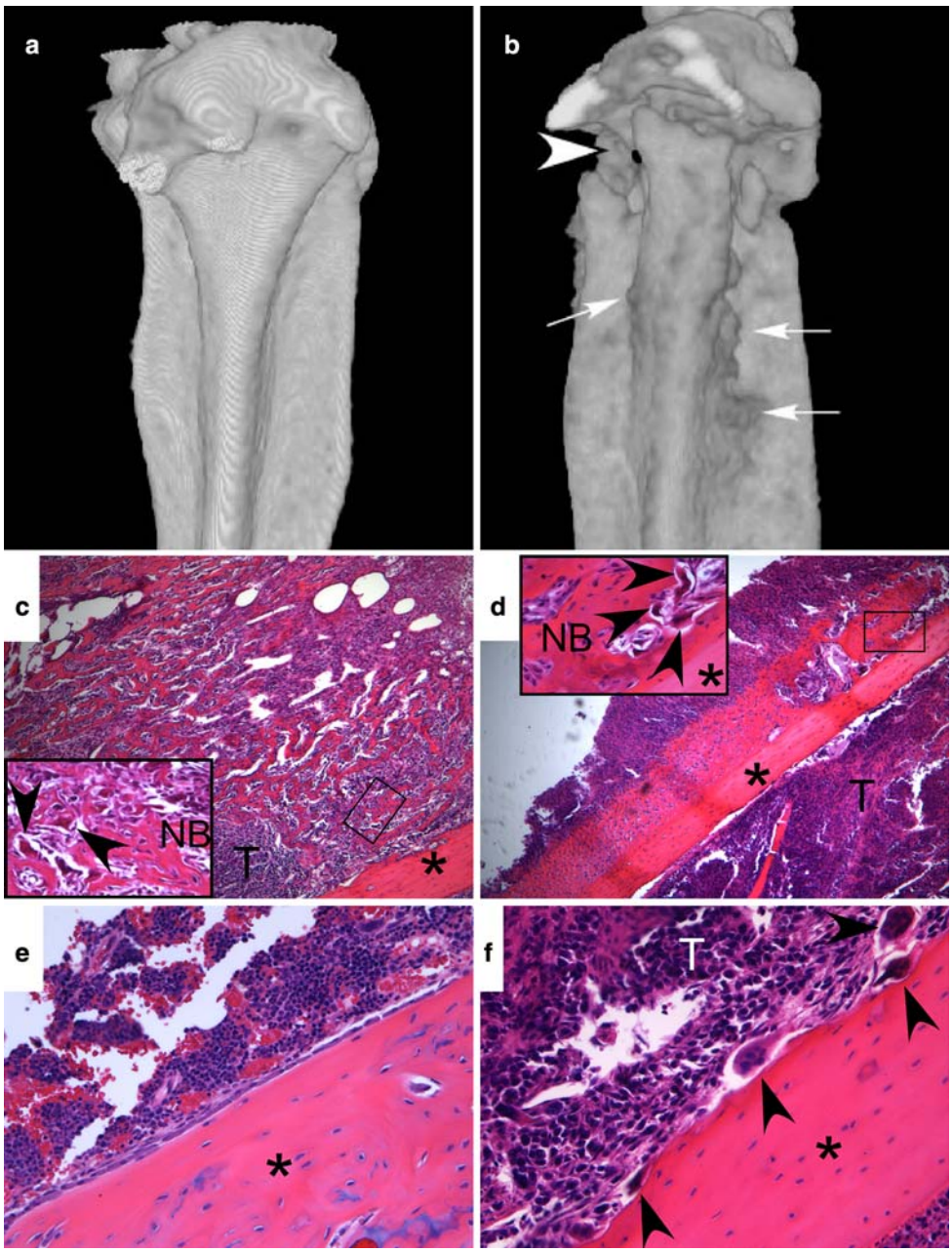

Fig. 3 RM1 cells promote extensive osteolysis leading to cortical breach and periosteal bone bone deposition. (**a**) and (**b**) 3D isosurface reconstructions of μCT data from the right tibiae of (**a**) a normal non-manipulated tibia and (**b**) a tibia 21 days following the injection of 1×10^3 RM1 cells. Tibiae are shown in a posterior-anterior view. Arrowhead indicates an area of extensive bone lysis. Arrows indicate regions of bone deposition. (**c**) and (**d**) are H&E stained sections illustrating different phenotypes of bone deposition. (**c**) Focus of new bone (NB) consisting of random, irregular periosteal networks adjacent to tumor (T). (**d**) Periosteal cortical thickening adjacent to tumor. Note the presence of osteoclasts (arrowheads) on the surface of newly deposited bone. (**e**) H&E stained section of PBS control injected tibia showing normal marrow and bone lining cells on the endosteal surface. (**f**) H&E stained section of RM1 injected tibia 10 days following implantation. Osteoclasts (arrowheads) recruited to the endosteal surface. Images of tissue sections were acquired at 5× (**c** and **d**) or 20× (**e** and **f**) magnification; insets are at 40× magnification. Asterisks indicate cortical bone

(early passage MC3T3-E1) cells. As shown in Fig. 5a, RM1 CCM enhanced the proliferation of MC3T3-E1 cells in a dose dependent manner. We next investigated the early steps of MC3T3-E1 differentiation by treatment with RM1 CCM. The presence of RM1 CCM together with OS medium promoted an increase in expression of both BSP (Fig. 5b and left panel 5c) and Collagen Iα1 (Fig. 5b and right panel 5c) over OS medium alone. In addition, surface expression of ALP was also elevated in the presence of OS and RM1 CCM (Fig. 5d) compared to OS medium alone. These data indicate that RM1 cells can promote the proliferation of the preosteoblastic MC3T3-E1 cells as well as increase the expression of early markers of osteoblast differentiation. Thus, our in vitro results support our μCT images by illustrating that RM1 cells have the potential for promoting both lytic and blastic bone responses and demonstrate the utility of RM1 bone cells in studies of tumor:bone stroma interactions.

Discussion

The use of human prostate cancer cells in mice to investigate tumor progression, metastasis, and interaction with host bone cells has proven invaluable in extracting potential factors involved in these processes; however, these

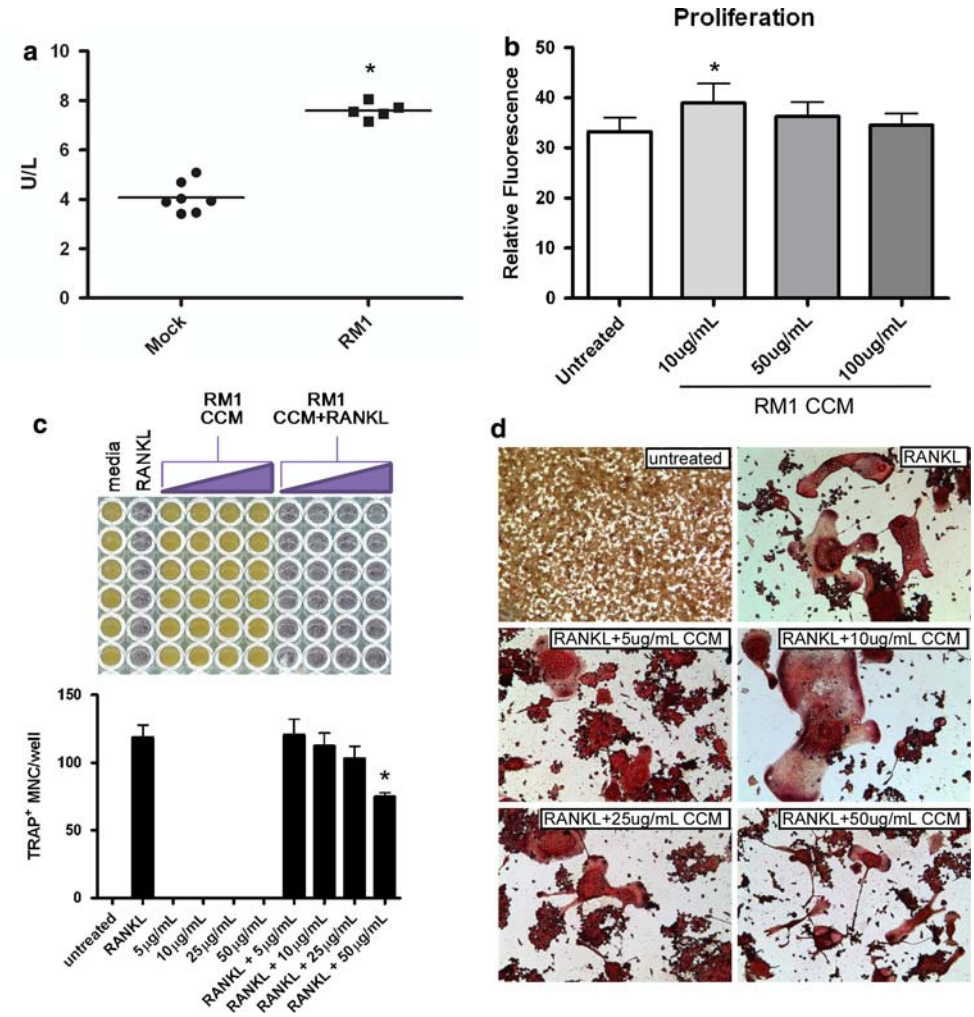

Fig. 4 Effects of RM1 cells on osteoclasts in vivo and on osteoclast precursor cells in vitro. (**a**) Serum TRAP levels two weeks following mock (PBS, $n = 7$) or RM1 cell (1×10^3, $n = 5$) intratibial injections. Line indicates the mean. (*) Compared to mock injected ($P \leq 0.05$). (**b**) Osteoclast precursor Raw264.7 cells 3 days following treatment with increasing concentrations of RM1 conditioned culture media (CCM). (*) Treatment (10 μg/ml) compared to untreated control ($P \leq 0.05$). (**c**) and (**d**) Differentiation of Raw264.7 cells in the presence of RANKL and RM1 cell CCM. (**c**) Raw264.7 cells stained for expression of TRAP (top) with total TRAP+ multinucleate cells (>3 nuclei) per well (bottom). Data represent average from 9 wells per group. (*) Treatment (RANKL + 50 μg/ml) compared to positive (RANKL) control ($P \leq 0.05$). (**d**) Representative images of wells from plate shown in (**c**). Graphs are mean ± SD

models are not without fault. First, the use of nude or SCID mice excludes the role of host immunity in the development of prostate cancer and secondary lesions. Second, the recognition of factors, such as growth factors or cell surface molecules, expressed/presented by host or prostate cancer cells may not be properly recognized by their cognate factors or receptors. Bone is known to be largely heterogeneous with regards to the cancellous or trabecular component and the milieus of bone microenvironments are largely dissimilar in human and mice. This is exemplified in studies where human prostate cancer cells demonstrate a preference for surgically implanted human bone fragments over that of their murine host [14]. Thus, it seems appropriate that the use of syngeneic tumor models deserves further attention. Unfortunately, the road to the development of new non-xenotransplant prostate cancer animal models is a slow one. One of the largest speed bumps in this road arises from the fact that mice inherently fail to develop prostate cancer. While several investigators have side-stepped this problem by developing models relying on the SV40 oncogene or conditional gene knockouts [4, 5, 7] which give clues to several facets of disease progression, there is a need for additional models to adequately describe the pathological condition in its entirety. One model, the mouse prostate reconstitution model, has garnered attention for use in immunotherapy studies of prostate cancer [9, 10]. Cell lines from this model arose through the introduction of activated oncogenes via retroviral infection of the mesenchymal urogenital sinus and subsequent engraftment under the renal capsule for tumor formation [8]. Herein, we describe the use of a cell line derived from the MPR model, the RM1 cell line, as a potentially effective model for investigating prostate cancer:bone stromal interactions in immune competent mice. To our knowledge, the introduction of RM1 cells into bone has been limited to studies investigating prostate cancer regulation of dendritic cell formation [15, 16].

We first chose to determine the most effective method of implantation that would yield reproducible skeletal lesions. To this end, we examined several well-characterized

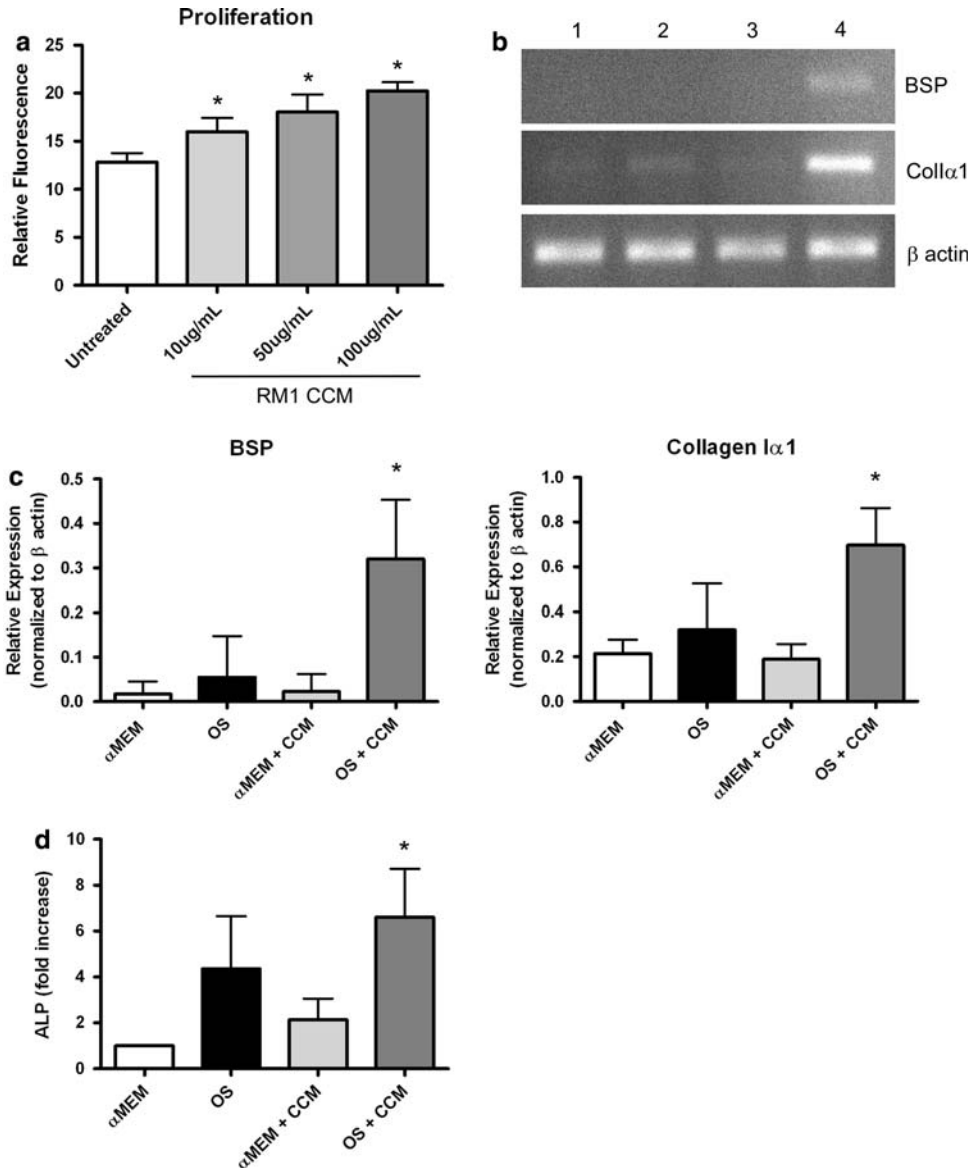

Fig. 5 Effects of RM1 cells on osteoblast precursor cells in culture. (**a**) Osteoblast precursor MC3T3-E1 cells 3 days following treatment with increasing concentrations of RM1 conditioned culture media (CCM). (*) Treatments compared to untreated control ($P \leq 0.05$). (**b**) Semi-quantitative RT-PCR of mRNA for genes involved in osteoblast differentiation from osteoblast precursor MC3T3-E1 cells. Results shown are representative of experimentation performed in triplicate. Treatments were as follows: (1) αMEM w/10% FBS, (2) OS medium (αMEM, 10%FBS, 50 μg ascorbate, 10 mM β-glycerol phosphate), (3) αMEM w/10% FBS and 50 μg/ml RM1 CCM, (4) OS medium with 50 μg/ml RM1 CCM. (**c**) Densitometric analysis of bands shown in (**b**). (*) OS + RM1 CCM compared to OS alone ($P \leq 0.05$). (**d**) Quantification of surface ALP expressed by MC3T3-E1 cells 5 days after initiation of treatments. Treatments were as in (**b**) except for reduced serum supplementation (2% FBS). Bars represent area of ALP positive cells of 10 fields from experiments completed in triplicate. (*) OS + RM1 CCM compared to OS alone ($P \leq 0.05$). All graphs are mean ± SD

injection techniques with increasing quantities of RM1 cells. We found that RM1 cells prefer direct intrabone implantation (100% incidence) compared to intracardiac injection or injection into the femoral artery (0% incidence). While the existence of micrometastases 21 days following RM1 intracardiac or femoral artery implantation cannot be excluded, the likelihood of this occurring is low due to the rapid expansion of these cells both in the subcutaneum (not shown) and after direct intrabone implantation. While direct injection to bone is not a true metastasis model and precludes insight into earlier steps of the metastatic process, information regarding late steps in the metastatic process, such as tumor growth/invasion within bone and tumor:bone stromal interactions, can be obtained. In the current study, tail vein injections were not examined since RM1 cell injection to the tail vein has previously been shown to yield massive lung metastases resulting in high mortality rates shortly following injection [17].

The progression of prostate cancer is usually considered a relatively slow process; unfortunately, this also slows the pace of investigations. The rapid growth of cells derived from the MPR model, while atypical of most patient derived cell lines, may prove beneficial in hastening discovery. By monitoring the formation of bone lesions longitudinally over a relatively short time period (20 days) using μCT evaluation, we were able to determine various time points associated with lesion development consisting of an early, injury induced blastic phase (around 5 days post insult; closure of injection site), osteolytic (between 5 and 15 days), and mixed responses (between 15 and 20 days). We have found that the late, minor blastic

response (post 15 days) induced by RM1 cells is confined to the periosteal region subsequent to cortical breach and invasion of adjacent soft tissue; a type of response noted in specific subsets of prostate cancer patients [18–21] as well as in several animal models utilizing cell lines from human [22] and canine [23] sources.

Following entrance into the skeletal compartment, prostate cancer cells participate in a reciprocating signaling relationship with bone stromal cells, previously characterized as a "vicious cycle" [24]. Facets of this cycle lead to the differentiation of osteoclast and osteoblast precursors as well as bone resorption and deposition by these differentiated cell types. It is obvious from our in vivo data that RM1 cells promote an osteolytic response following growth in bone, while in vitro data indicates enhanced proliferation of osteoclast precursors with little effect on differentiation except at high concentrations of RM1 conditioned culture medium where the number of multinucleate TRAP expressing cells decreased. Our in vivo images also depicted periosteal bone deposition post RM1 corticle breach. Although we cannot conclude that the observed periosteal bone formation found in vivo following RM1 intraosseous implantation is not a secondary reaction due to marked lysis and tibial instability, direct intratibial implantation of a syngeneic breast cancer cell line elicits a strictly lytic response (Supplemental Fig. 1) in the face of corticle breach and periosteal tumor expansion. Furthermore our in vitro findings indicate that RM1 cells can promote early expression of BSP, collagen Iα1, and surface expression of ALP, factors typically used to assess osteoblast differentiation. Our data illuminates some similarities between RM1 cells and the human prostate cancer line PC3; a highly lytic cell line [25] shown to promote osteoblast precursor proliferation [26]. However, RM1 cells, in contrast to PC3 cells, have the potential to promote in vivo bone deposition following intraosseous implantation while PC-3 lesions are strictly lytic.

Animal models that faithfully recapitulate human disease are in high demand considering the treatment difficulties associated with bone metastatic prostate cancer. Using murine RM1 PCa cells and direct intraosseous injections, we illustrate the potential of RM1 cells as a new tool for investigating prostate cancer:bone stroma interactions and associated lytic and osteoblastic responses. The described model allows the study of both lytic and blastic responses accompanied by an accelerated pace of discovery and the ability to study disease in immune competent/transgenic C57BL/6 hosts. We feel that this model could prove invaluable in the field of prostate cancer research.

Acknowledgements This work was supported by the following grants: DK060933/CA126847 to T.V. Byzova. N.P. McCabe is supported by a Ruth L. Kirschstein Research Service Award (NRSA) Individual Fellowship (5F32CA1172462); Cleveland Clinic Musculoskeletal Core Center funded in part by NIAMS Core Center Grant 1P30 AR-050953.

References

1. American Cancer Society (2007) Cancer facts & figures 2007. American Cancer Society, Inc., Atlanta
2. Coleman RE (1997) Skeletal complications of malignancy. Cancer 80:1588–1594. doi:10.1002/(SICI)1097-0142(19971015)80:8±≤1588::AID-CNCR9≥3.0.CO;2-G
3. Keller ET, Brown J (2004) Prostate cancer bone metastases promote both osteolytic and osteoblastic activity. J Cell Biochem 91:718–729. doi:10.1002/jcb.10662
4. Greenberg NM, DeMayo F, Finegold MJ, Medina D, Tilley WD, Aspinall JO, Cunha GR, Donjacour AA, Matusik RJ, Rosen JM (1995) Prostate cancer in a transgenic mouse. Proc Natl Acad Sci USA 92:3439–3443. doi:10.1073/pnas.92.8.3439
5. Kasper S, Sheppard PC, Yan Y, Pettigrew N, Borowsky AD, Prins GS, Dodd JG, Duckworth ML, Matusik RJ (1998) Development, progression, and androgen-dependence of prostate tumors in probasin-large T antigen transgenic mice: a model for prostate cancer. Lab Invest 78:319–333
6. Wu X, Wu J, Huang J, Powell WC, Zhang J, Matusik RJ, Sangiorgi FO, Maxson RE, Sucov HM, Roy-Burman P (2001) Generation of a prostate epithelial cell-specific Cre transgenic mouse model for tissue-specific gene ablation. Mech Dev 101:61–69. doi:10.1016/S0925-4773(00)00551-7
7. Di Cristofano A, Pesce B, Cordon-Cardo C, Pandolfi PP (1998) Pten is essential for embryonic development and tumour suppression. Nat Genet 19:348–355. doi:10.1038/1235
8. Thompson TC, Southgate J, Kitchener G, Land H (1989) Multistage carcinogenesis induced by ras and myc oncogenes in a reconstituted organ. Cell 56:917–930. doi:10.1016/0092-8674(89)90625-9
9. Grant JF, Iwasawa T, Sinn HW, Siemens DR, Griffith TS, Takacs EB, Ratliff TL (2006) Induction of protective immunity to RM-1 prostate cancer cells with ALVAC-IL-2/IL-12/TNF-alpha combination therapy. Int J Cancer 119:2632–2641. doi:10.1002/ijc.22220
10. Griffith TS, Kawakita M, Tian J, Ritchey J, Tartaglia J, Sehgal I, Thompson TC, Zhao W, Ratliff TL (2001) Inhibition of murine prostate tumor growth and activation of immunoregulatory cells with recombinant canarypox viruses. J Natl Cancer Inst 93:998–1007. doi:10.1093/jnci/93.13.998
11. Hall SJ, Thompson TC (1997) Spontaneous but not experimental metastatic activities differentiate primary tumor-derived vs metastasis-derived mouse prostate cancer cell lines. Clin Exp Metastasis 15:630–638. doi:10.1023/A:1018499515883
12. Baley PA, Yoshida K, Qian W, Sehgal I, Thompson TC (1995) Progression to androgen insensitivity in a novel in vitro mouse model for prostate cancer. J Steroid Biochem Mol Biol 52:403–413. doi:10.1016/0960-0760(95)00001-G
13. Rozen S, Skaletsky H (2000) Primer3 on the WWW for general users and for biologist programmers. Methods Mol Biol 132:365–386
14. Yonou H, Yokose T, Kamijo T, Kanomata N, Hasebe T, Nagai K, Hatano T, Ogawa Y, Ochiai A (2001) Establishment of a novel species- and tissue-specific metastasis model of human prostate cancer in humanized non-obese diabetic/severe combined immunodeficient mice engrafted with human adult lung and bone. Cancer Res 61:2177–2182
15. Tourkova IL, Yamabe K, Chatta G, Shurin GV, Shurin MR (2003) NK cells mediate Flt3 ligand-induced protection of dendritic cell

precursors in vivo from the inhibition by prostate carcinoma in the murine bone marrow metastasis model. J Immunother (1997) 26:468–472
16. Tourkova IL, Yamabe K, Foster B, Chatta G, Perez L, Shurin GV, Shurin MR (2004) Murine prostate cancer inhibits both in vivo and in vitro generation of dendritic cells from bone marrow precursors. Prostate 59:203–213. doi:10.1002/pros.10369
17. Voeks DJ, Martiniello-Wilks R, Russell PJ (2002) Derivation of MPR and TRAMP models of prostate cancer and prostate cancer metastasis for evaluation of therapeutic strategies. Urol Oncol 7:111–118. doi:10.1016/S1078-1439(01)00180-6
18. Bloom RA, Libson E, Husband JE, Stoker DJ (1987) The periosteal sunburst reaction to bone metastases. A literature review and report of 20 additional cases. Skeletal Radiol 16:629–634. doi:10.1007/BF00357111
19. El Otmany A, Bouklata S, Hafid H, Chami I, Jalil A, Benjelloun S, Souadka A, Belabbas M (2000) Bone metastasis revealing a primary prostate cancer. J Radiol 81:990–991
20. Hove B, Gyldensted C (1990) Spiculated vertebral metastases from prostatic carcinoma. Report of first two cases. Neuroradiology 32:337–339. doi:10.1007/BF00593059
21. Wyche LD, de Santos LA (1978) Spiculated periosteal reaction in metastatic disease resembling osteosarcoma. Orthopedics 1: 215–221
22. Henry MD, Silva MD, Wen S, Siebert E, Solin E, Chandra S, Worland PJ (2005) Spiculated periosteal response induced by intraosseous injection of 22Rv1 prostate cancer cells resembles subset of bone metastases in prostate cancer patients. Prostate 65:347–354. doi:10.1002/pros.20300
23. LeRoy BE, Bahnson RR, Rosol TJ (2002) New bone formation in nude mouse calvaria induced by canine prostate tissue. Mol Cell Endocrinol 197:257–263. doi:10.1016/S0303-7207(02)00260-5
24. Chirgwin JM, Mohammad KS, Guise TA (2004) Tumor-bone cellular interactions in skeletal metastases. J Musculoskelet Neuronal Interact 4:308–318
25. Corey E, Quinn JE, Bladou F, Brown LG, Roudier MP, Brown JM, Buhler KR, Vessella RL (2002) Establishment and characterization of osseous prostate cancer models: intra-tibial injection of human prostate cancer cells. Prostate 52:20–33. doi:10.1002/pros.10091
26. Martinez J, Silva S, Santibanez JF (1996) Prostate-derived soluble factors block osteoblast differentiation in culture. J Cell Biochem 61:18–25. doi:10.1002/(SICI)1097-4644(19960401)61:1≤18::AID-JCB3≥3.0.CO;2-5